Temperature variance and turbulent kinetic energy as potentials of the inhomogeneous dissipation

I. Otić

Karlsruhe Institute of Technology (KIT), Hermann-von-Helmholtz-Platz 1, 76344 Eggenstein-Leopoldshafen, Germany

ivan.otic@kit.edu

Abstract. The two-point decomposition of the dissipation rates identifies the Laplacians of the temperature variance $\overline{\theta^2}$ and of the turbulent kinetic energy k with the inhomogeneous parts of the respective dissipation rates, $\Delta_x \overline{\theta^2} = 4\varepsilon_{\theta,ih}/\kappa$ and $\Delta_x k = 2\varepsilon_{ih}/\nu$. By Green's third identity both fields are therefore represented exactly, in any flow domain, as boundary terms plus Newtonian potentials of the inhomogeneous dissipations. At isothermal no-slip boundaries the boundary terms vanish and the complete $\overline{\theta^2}$ and k fields are potentials of the inhomogeneous parts of their own dissipation rates. At boundaries with fluctuating temperature the wall variance enters as boundary value. The representation is kinematic, with no transport equation entering its derivation, and it contains no adjustable constant. The dynamics of the variance transport, including the mechanism sustaining the turbulence, acts on the variance fields only through the inhomogeneous dissipations. The representation is the exact, parameter-free counterpart of the elliptic-relaxation structure of near-wall turbulence closures. Channel-flow direct numerical simulation data at $Pr = 0.71$, 0.025 and 0.01 under isothermal, imposed-flux, Robin and conjugate thermal conditions reproduce the representation to 0.1% on wall-resolved data at isothermal walls, and to a few percent where the wall variance enters as boundary value or the wall is not resolved. An a priori reconstruction from published variance profiles traces the sweep from shear-driven mixed convection to the Rayleigh–Bénard limit, in which the bulk is harmonic. The inhomogeneous fractions $f_\theta = \varepsilon_{\theta,ih}/\varepsilon_\theta$ and $f_u = \varepsilon_{ih}/\varepsilon$ measure the departure of the variance fields from harmonicity, and the representation provides an exact consistency condition for turbulence closures and data-driven models.

1 Introduction

The transport equations for the temperature variance $\overline{\theta^2}$ and the turbulent kinetic energy k are central to turbulent heat-transfer theory and modeling, see e.g. Corrsin [1], Launder [2]. In the preceding analysis [3] the two-point correlation technique of Chou [4] and Burgers [5], applied to the kinetic-energy dissipation by Kolovandin and Vatutin [6] and Jovanović et al. [7], was extended to the dissipation rate ε_θ of the temperature variance: the exact decomposition $\varepsilon_\theta = \varepsilon_{\theta,h} + \varepsilon_{\theta,ih}$, with the inhomogeneous part $\varepsilon_{\theta,ih} = \frac{1}{4}\kappa\Delta_x\overline{\theta^2}$ absorbed by molecular diffusion in the variance transport equation, leaves the homogeneous part as the only dissipation quantity requiring closure and yields exact near-wall results for the thermal-to-mechanical time-scale ratio.

The present paper develops a direct consequence of those results. The defining relations identify the Laplacians of $\overline{\theta^2}$ and k with the inhomogeneous dissipation parts. Green's third identity then represents both fields exactly, in any flow domain, as boundary terms plus Newtonian potentials of $\varepsilon_{\theta,ih}$ and ε_{ih} (§2). At isothermal no-slip boundaries the boundary terms vanish, and the complete variance fields are potentials of the inhomogeneous parts of their own dissipation rates. At boundaries with fluctuating temperature the wall variance enters as boundary value.

The representation is kinematic. It follows from the two-point identities and from Green's identity alone, and no transport equation is used in its derivation. The dynamics of the variance transport enters through the fields themselves: the transport equations and the mechanism sustaining the turbulence determine the inhomogeneous dissipations, and the representation expresses the variance fields as boundary terms plus potentials of these dissipations.

In this respect it stands with the Biot–Savart integral, which determines the velocity field kinematically from the vorticity, and with the Poisson integral for the fluctuating pressure, which underlies the nonlocal analysis of the redistribution by Chou [4]. Such kinematic statements locate the dynamical content of the transport. In this formulation it resides in the inhomogeneous dissipations. The representation makes exact, for the variance fields, a structure long employed in near-wall closure modeling. The elliptic relaxation of Durbin [8, 9] encodes the wall-induced nonlocality of the pressure–strain redistribution through a modeled elliptic equation with a prescribed length scale. The idea has been adopted in various forms, e.g. the elliptic-blending closure of Manceau and Hanjalić [10], its extension to turbulent natural and mixed convection by Kenjereš et al. [11], and the elliptic-blending model for near-wall, separated and buoyant flows of Billard and Laurence [12]. The analogy concerns the structure, not the quantity represented. The elliptic-relaxation equation is a model for the redistribution. The present representation is an exact statement about the variance fields themselves, with a parameter-free kernel and the inhomogeneous dissipation as source.

The result is general. It is most directly evaluated in statistically one-dimensional flows, where the kernel is explicit. Section 3 performs this evaluation on channel-flow DNS data from three independent codes at $Pr = 0.71$, 0.025 and 0.01, under isothermal, imposed-flux, Robin and conjugate thermal conditions, and, as an a priori reconstruction from published variance profiles, on mixed convection and on the Rayleigh–Bénard limit, tracing the approach to the harmonic bulk. Section 4 collects the consequences: the inhomogeneous fractions [3, 6, 7] as measures of the departure from harmonicity, an exact consistency condition for turbulence closures and data-driven models.

2 Exact integral representation

With the Reynolds decompositions $U_i = \overline{U_i} + u_i$, $T = \overline{T} + \theta$, the $\xi \to 0$ limit of the two-point correlation equations, with ξ the separation vector, gives the exact decompositions [3, 6, 7]

$$\varepsilon_\theta = \varepsilon_{\theta,h} + \varepsilon_{\theta,ih}, \quad \varepsilon_{\theta,ih} = \tfrac{1}{4}\kappa\,\Delta_x\overline{\theta^2}; \qquad \varepsilon = \varepsilon_h + \varepsilon_{ih}, \quad \varepsilon_{ih} = \tfrac{1}{2}\nu\,\Delta_x k, \tag{1}$$

with Δ_x the Laplacian, κ the thermal diffusivity and ν the kinematic viscosity. Green's third identity [see e.g. 13] then gives, for any point x of a flow domain V with boundary S, $r = |x - x'|$ and outward normal derivative ∂_n,

$$\overline{\theta^2}(x) = \frac{1}{4\pi}\oint_S \left[\frac{1}{r}\,\partial_n\overline{\theta^2} - \overline{\theta^2}\,\partial_n\frac{1}{r}\right] \mathrm{d}S \;-\; \frac{1}{\pi\kappa}\int_V \frac{\varepsilon_{\theta,ih}(x')}{r}\,\mathrm{d}V', \tag{2}$$

$$k(x) = \frac{1}{4\pi}\oint_S \left[\frac{1}{r}\,\partial_n k - k\,\partial_n\frac{1}{r}\right] \mathrm{d}S \;-\; \frac{1}{2\pi\nu}\int_V \frac{\varepsilon_{ih}(x')}{r}\,\mathrm{d}V'. \tag{3}$$

Equations (2)–(3) hold without any assumption on the flow: the variance fields are boundary terms plus the Newtonian potentials of the inhomogeneous dissipations. As mathematics the representation is immediate, since (1) is a Poisson problem for the variance fields. Its content is physical. The inhomogeneous dissipations are confined essentially to the wall layers [3], so the representation states that the variance fields are set by the wall-layer inhomogeneous dissipation and transmitted nonlocally by the kernel. At an isothermal no-slip boundary $k = 0 = \overline{\theta^2}$. If the free-space kernel in (2)–(3) is replaced by the Green function of the domain with homogeneous Dirichlet condition, the normal-derivative boundary terms are eliminated, and only the boundary values of $\overline{\theta^2}$ and k remain in the representation. In a domain bounded by isothermal no-slip walls these vanish, and

$$\overline{\theta^2}(x) = -\frac{4}{\kappa}\int_V G_D(x,x')\,\varepsilon_{\theta,ih}(x')\,\mathrm{d}V', \qquad k(x) = -\frac{2}{\nu}\int_V G_D(x,x')\,\varepsilon_{ih}(x')\,\mathrm{d}V', \tag{4}$$

with G_D the Dirichlet Green function of the domain: the $\overline{\theta^2}$ and k fields are potentials of the inhomogeneous parts of their own dissipation rates. At boundaries with fluctuating temperature (imposed-flux, Robin, conjugate), $\overline{\theta^2}$ does not vanish, and its boundary values enter (4) through the standard boundary integral of the Dirichlet problem: the wall variance enters the representation as boundary value, the same quantity that sets the singular near-wall amplitudes of the time-scale ratios in [3]. Three consequences follow. (i) The inhomogeneous parts determine the variance fields. Positivity of $\overline{\theta^2}$ and k, together with the positivity of the Dirichlet kernel, requires the kernel-weighted integrals of $\varepsilon_{\theta,ih}$ and ε_{ih} in (4) to be negative at every point. The inhomogeneous parts therefore cannot be single-signed. Their sign structure is a consequence of the representation, not an incidental feature of the data. (ii) Every moment of the variance fields is an integral of the inhomogeneous dissipations against a kernel. (iii) A modeled $\overline{\theta^2}$ or k field is fixed by its modeled dissipation decomposition together with the wall data, so that a closure cannot prescribe profile and split independently.

In a statistically one-dimensional flow, as in fully developed channel flow or in Rayleigh–Bénard convection, the representation reduces to an explicit form. On the normalized layer $0 \le x_3 \le 1$ between the walls, the Dirichlet Green function is $G_D(x_3,x_3') = \min(x_3,x_3')\,[1 - \max(x_3,x_3')]$, and for a symmetric half-layer $0 \le y \le h$ with symmetry at $y = h$, $G_D(y,y') = \min(y,y')$. Between isothermal no-slip walls,

$$\overline{\theta^2}(x_3) = -\frac{4}{\kappa}\int_0^1 G_D(x_3,x_3')\,\varepsilon_{\theta,ih}(x_3')\,\mathrm{d}x_3', \qquad k(x_3) = -\frac{2}{\nu}\int_0^1 G_D(x_3,x_3')\,\varepsilon_{ih}(x_3')\,\mathrm{d}x_3', \tag{5}$$

and at a wall with fluctuating temperature the boundary integral reduces to the additive constant $\overline{\theta^2}_w$,

$$\overline{\theta^2}(y) \;=\; \overline{\theta^2}_w \;-\; \frac{4}{\kappa}\int_0^h \min(y,y')\,\varepsilon_{\theta,ih}(y')\,\mathrm{d}y'. \tag{6}$$

Equations (5)–(6) are evaluated directly on channel-flow DNS data in §3.

The harmonic limit of (2)–(3) orders the flow regimes. On the set $M_\delta = \{x : |f_\theta| < \delta,\ |f_u| < \delta\}$, with $f_\theta = \varepsilon_{\theta,ih}/\varepsilon_\theta$ and $f_u = \varepsilon_{ih}/\varepsilon$ the inhomogeneous fractions, the volume terms are smaller by $O(\delta)$ than the potentials of the full dissipations. The fields are harmonic to that order and are determined by their values on ∂M_δ, the boundary-layer edge. The fractions are thus quantitative measures of the departure from harmonicity. The production terms are not such measures: harmonicity concerns the molecular diffusion of the variances, and vanishing production does not imply vanishing Laplacians, nor does the converse hold. In a statistically one-dimensional configuration the harmonic solutions are linear profiles, and the solution compatible with midplane symmetry is a constant, so the constancy of the bulk statistics observed in strongly buoyancy-driven convection is not merely consistent with the harmonic limit but is the harmonic solution itself. Rayleigh–Bénard convection is the limiting configuration of this kind: the mean velocity vanishes identically, at sufficiently high Rayleigh number the mean-temperature gradient vanishes in the bulk, the molecular diffusion of the variances is negligible there, the fractions are small, and the variance fields are harmonic, determined by the boundary-layer inhomogeneous contributions transmitted nonlocally, see e.g. Otić et al. [14]. The coincidence of vanishing production and vanishing fractions is a property of this limit, not of the representation, which covers the non-harmonic regimes evaluated next: the forced channel is the strongly non-harmonic case, and mixed convection interpolates between the two.

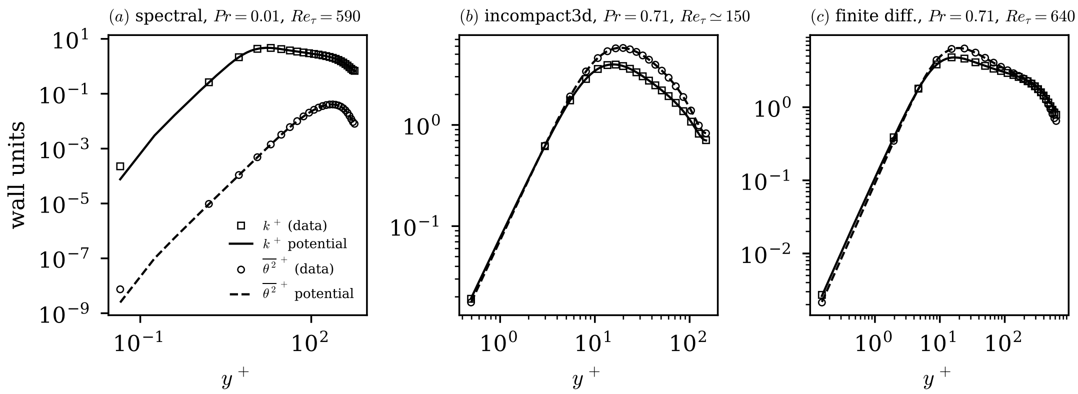

Figure 1: Potential representation (5) in isothermal channel flow, wall units: k^+ and $\overline{\theta^2}^+$ from the DNS (symbols) and the potentials of ε_{ih} and $\varepsilon_{\theta,ih}$ (lines). (*a*) Pseudo-spectral data, $Pr = 0.01$, $Re_\tau = 590$ [15]. (*b*) incompact3d data, $Pr = 0.71$, $Re_\tau \simeq 150$ [16]. (*c*) finite-difference data, $Pr = 0.71$, $Re_\tau = 640$ [17].

3 Evaluation on channel-flow DNS data

Three channel-flow databases are used for the evaluation. The pseudo-spectral simulations of Tiselj and Cizelj [15] cover $Pr = 0.01$ at $Re_\tau = 180$, 395 and 590 and store the wall point. The sixth-order compact-finite-difference simulations with incompact3d of Flageul et al. [16] cover $Pr = 0.71$ under Dirichlet, Neumann, Robin and conjugate thermal conditions. The finite-difference simulations of Abe et al. [17] cover $Pr = 0.71$ and 0.025.

The inhomogeneous parts are taken from the dissipation and budget statistics of the databases. These statistics are accumulated from the fluctuating gradient fields during the simulations and are therefore independent of the variance profiles against which the representation is tested. Equation (1) sets their wall-unit form, with primes denoting derivatives with respect to y^+: $k'' = 2\varepsilon_{ih}$ and $\overline{\theta^2}'' = 4Pr\,\varepsilon_{\theta,ih}$.

For the isothermal cases, figure 1 compares the DNS profiles of k^+ and $\overline{\theta^2}^+$ with the potentials (5). Agreement is quantified below by the core-median ratio, the median over the channel core $30 \le y^+ \le 0.8\,Re_\tau$, of the pointwise ratio of the DNS profile to the representation.

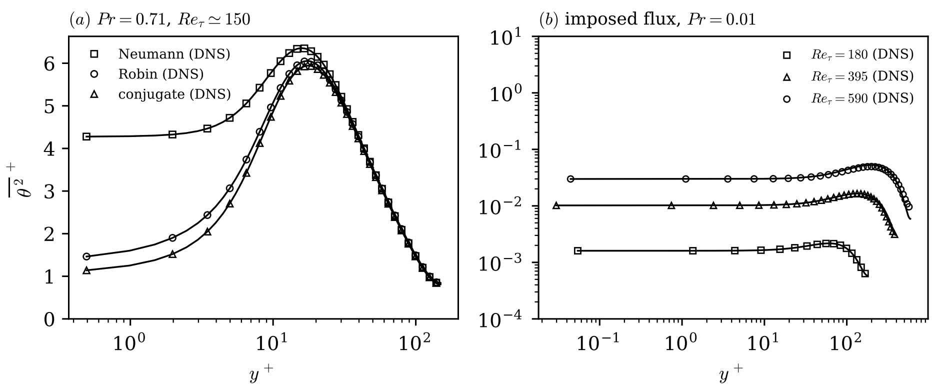

Figure 2: Representation (6) at walls with fluctuating temperature, wall units: $\overline{\theta^2}^+$ from the DNS (symbols) and the representation (lines). (*a*) Neumann, Robin and conjugate walls, $Pr = 0.71$ [16]. (*b*) imposed-flux walls, $Pr = 0.01$, $Re_\tau = 180$, 395 and 590 [15].

The representation reproduces both profiles with core-median ratios 0.999–1.001 in the spectral cases at all three Reynolds numbers and in the incompact3d case, within the statistical quality of the data, and $\approx$ 0.98 in the finite-difference cases, whose first grid point lies at $y^+ \approx 0.15$ and whose coarser budget resolution accounts for the residual.

For walls with fluctuating temperature, the form (6) is evaluated with $\overline{\theta^2}_w$ taken from the data. Figure 2 compares the DNS profiles with the representation for the Neumann, Robin and conjugate cases of Flageul et al. [16] and for the imposed-flux cases of Tiselj and Cizelj [15]. The core-median ratios are 0.998–1.002 for the Neumann, Robin and conjugate walls and 0.957–1.000 for the imposed-flux walls at $Re_\tau = 180$–590. The larger deviations of the imposed-flux cases reflect the wall variance $\overline{\theta^2}_w$, which enters as additive constant and carries the statistical uncertainty of the wall statistics directly into the representation. The turbulent kinetic energy satisfies the potential form (5) at all wall types, with ratios 0.995–1.003.

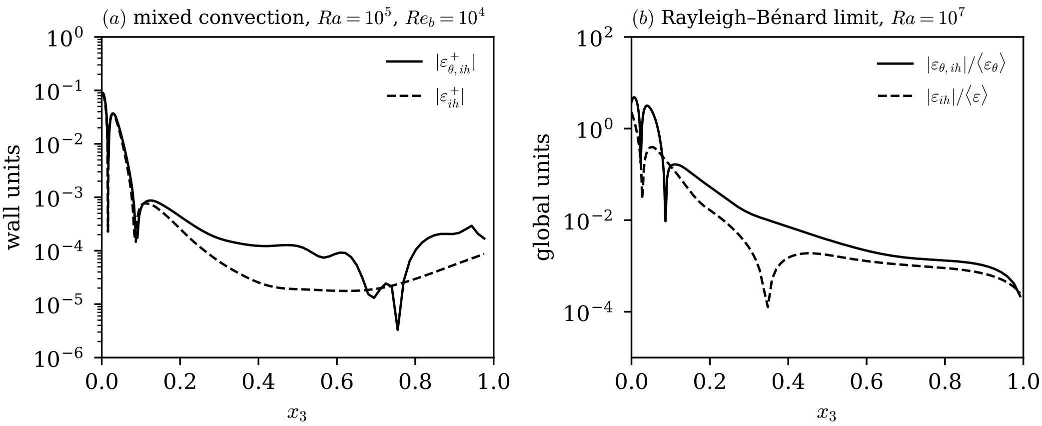

Figure 3: A priori reconstruction of the inhomogeneous dissipation parts from the variance profiles of Pirozzoli et al. [18]. (*a*) Mixed-convection case at $Ra = 10^5$, $Re_b = 10^4$, wall units. (*b*) Rayleigh–Bénard limit at $Ra = 10^7$, $Pr = 1$, normalized by the global dissipation rates from the exact relations. Lower half of the layer, with x_3 in units of the half height.

The representation applies also to data sets that provide the variance profiles but no dissipation statistics, as an a priori reconstruction in the sense of [3]: equation (1) determines the inhomogeneous parts directly from the profiles.

The published profiles are differentiated on their original grids with a quintic smoothing spline. The reconstruction is a diagnostic of the data and not a test of the representation, since the source is here computed from the profile itself. Figure 3 shows this reconstruction for two cases of Pirozzoli et al. [18], which span, in the same geometry, the sweep from shear-driven to buoyancy-driven convection: a mixed-convection case at $Ra = 10^5$ and bulk Reynolds number $Re_b = 10^4$ ($Re_\tau \simeq 300$), and the Rayleigh–Bénard limit at $Ra = 10^7$, $Pr = 1$. Both configurations have fixed wall temperatures, so the pure potential form (5) applies without a wall-variance term. The Rayleigh–Bénard case is normalized by the exact global relations $\langle\varepsilon\rangle = (\nu^3/H^4) Ra\, Pr^{-2}(Nu - 1)$ and $\langle\varepsilon_\theta\rangle = \kappa(\Delta T/H)^2 Nu - \kappa\langle(\mathrm{d}\overline{T}/\mathrm{d}x_3)^2\rangle$ [19, 20], with $\langle\cdot\rangle$ denoting the ensemble average and with Nu and the mean-gradient term evaluated from the mean-temperature profile. The cited relation holds for the total temperature gradient, and the subtracted term isolates the fluctuation dissipation ε_θ. These relations are restricted to the Rayleigh–Bénard limit: in the mixed case the mean-shear production contributes to the global kinetic-energy balance, and the case is therefore presented in wall units. In both cases the inhomogeneous parts are confined to the boundary layers. In the Rayleigh–Bénard limit their bulk values are 1.5–5.4 $\times 10^{-3}$ of the global dissipation rates: the bulk is harmonic to within one percent, consistent with the vanishing mean-temperature gradient there.

In the mixed case the bulk values are 1.2×10^{-4} ($\varepsilon_{\theta,ih}$) and 2.3×10^{-5} (ε_{ih}) in wall units, three to four orders of magnitude below the wall-layer maxima. Referred to the mean fluctuation dissipation obtained from the exact wall-units heat balance, the thermal bulk value corresponds to 2–3 $\times 10^{-3}$ of $\langle \varepsilon_\theta \rangle$. This is the same order as in the Rayleigh–Bénard limit. At these parameters the bulk is harmonic across the sweep from shear-driven to buoyancy-driven convection.

4 Summary

The two-point decomposition of the dissipation rates implies, through Green's third identity, an exact integral representation of the temperature variance and the turbulent kinetic energy in an arbitrary flow domain: boundary terms plus Newtonian potentials of the inhomogeneous dissipation parts, with no adjustable constant and no reference to the mechanism sustaining the turbulence, which affects the fields only through the dissipations themselves. At isothermal no-slip boundaries the fields are potentials of the inhomogeneous parts of their own dissipation rates, equation (4). At boundaries with fluctuating temperature the wall variance enters as boundary value. The representation is the exact, parameter-free counterpart of the elliptic-relaxation structure of near-wall closures [8–12]. Channel-flow DNS data from three independent codes, at three Prandtl numbers and under four thermal boundary conditions, reproduce the representation to 0.1% at isothermal walls where the data resolve the wall, and to a few percent where the wall variance enters as boundary value or the wall is not resolved, and the a priori reconstruction on the mixed and Rayleigh–Bénard cases traces the approach to the harmonic bulk.

Three consequences follow. First, the representation is an exact consistency condition for turbulence closures: a modeled variance field is fixed by its modeled dissipation decomposition together with the wall data, a constraint of the same character as the invariance results of Pope [21] employed in data-driven modeling by Ling et al. [22], and complementary to the constraints [3, 23]. Second, the inhomogeneous fractions f_θ and f_u are quantitative measures of the departure from harmonicity. Along the sweep from forced channel flow through mixed convection to the Rayleigh–Bénard limit the bulk fractions decrease, and in the limit the variance fields are determined by boundary-layer-edge data alone. Third, because the representation connects independently computed quantities without adjustable constants, it provides a parameter-free consistency check for the processing and normalization of DNS data sets, and an a priori reconstruction of the inhomogeneous dissipation parts for data sets that report no dissipation statistics. Ongoing work addresses the budget-resolved analysis of the buoyancy-driven limit on the basis of dedicated wall-resolved simulations, and the extension to conjugate configurations, in which the wall variance becomes a property of the wall material and thickness.

Acknowledgments

This study was supported by Technological Research Council of Türkiye (TÜBİTAK), Project No. 123M535, and by the European Union co-funded partnership CONNECT-NM under Grant Agreement No. 101165375. The channel-flow data of Abe, Kawamura and co-workers were obtained from the JAXA DNS database. The data of Flageul and co-workers were obtained from the public repository of the Jožef Stefan Institute. The data of Pirozzoli and co-workers were obtained from the public repository of Sapienza Università di Roma. The $Pr = 0.01$ database was kindly provided by I. Tiselj. The author reports no conflict of interest.

Data availability

The DNS databases analyzed here are available from the JAXA DNS database [17], from the repository repo.ijs.si/CFLAG/incompact3d [16], from the repository http://newton.dma.uniroma1.it/mixconv/ [18] and from the authors of Tiselj and Cizelj [15]. The processing scripts and derived profiles are available from the author on reasonable request.

References

[1] S. Corrsin. The decay of isotropic temperature fluctuations in an isotropic turbulence. *J. Aeronaut. Sci.*, 18:417–423, 1951. doi: 10.2514/8.1982.

[2] B. E. Launder. On the computation of convective heat transfer in complex turbulent flows. *Trans. ASME J. Heat Transfer*, 110:1112–1128, 1988. doi: 10.1115/1.3250614.

[3] I. Otić. A homogeneous thermal-to-mechanical time-scale ratio and its near-wall behavior. KITopen preprint, Karlsruhe Institute of Technology, 2026. URL https://publikationen.bibliothek.kit.edu/1000195654. Published 27 July 2026; submitted to Phys. Rev. Fluids.

[4] P. Y. Chou. On velocity correlations and the solutions of the equations of turbulent fluctuation. *Quart. Appl. Math.*, 3:38–54, 1945. doi: 10.1090/qam/11999.

[5] J. M. Burgers. Some considerations on turbulent flow with shear. In *Proc. K. Ned. Akad. Wet., Ser. B*, volume 6, pages 125–147, 1953.

[6] B. A. Kolovandin and I. A. Vatutin. Statistical transfer theory in non-homogeneous turbulence. *Int. J. Heat Mass Transfer*, 15:2371–2383, 1972. doi: 10.1016/0017-9310(72)90133-0.

[7] J. Jovanović, Q.-Y. Ye, and F. Durst. Statistical interpretation of the turbulent dissipation rate in wall-bounded flows. *J. Fluid Mech.*, 293:321–347, 1995. doi: 10.1017/S002211209500173X.

[8] P. A. Durbin. Near-wall turbulence closure modeling without "damping functions". *Theor. Comput. Fluid Dyn.*, 3:1–13, 1991. doi: 10.1007/BF00271513.

[9] P. A. Durbin. A Reynolds stress model for near-wall turbulence. *J. Fluid Mech.*, 249:465–498, 1993. doi: 10.1017/S0022112093001259.

[10] R. Manceau and K. Hanjalić. Elliptic blending model: A new near-wall Reynolds-stress turbulence closure. *Phys. Fluids*, 14:744–754, 2002. doi: 10.1063/1.1432693.

[11] S. Kenjereš, S. B. Gunarjo, and K. Hanjalić. Contribution to elliptic relaxation modelling of turbulent natural and mixed convection. *Int. J. Heat Fluid Flow*, 26(4):569–586, 2005. doi: 10.1016/j.ijheatfluidflow.2005.03.007.

[12] F. Billard and D. Laurence. A robust k–ε–$\overline{v^2}/k$ elliptic blending turbulence model applied to near-wall, separated and buoyant flows. *Int. J. Heat Fluid Flow*, 33(1):45–58, 2012. doi: 10.1016/j.ijheatfluidflow.2011.11.003.

[13] F. John. *Partial Differential Equations.* Springer, 3 edition, 1978.

[14] I. Otić, G. Grötzbach, and M. Wörner. Analysis and modelling of the temperature variance equation in turbulent natural convection for low-Prandtl-number fluids. *J. Fluid Mech.*, 525:237–261, 2005. doi: 10.1017/S0022112004002733.

[15] I. Tiselj and L. Cizelj. DNS of turbulent channel flow with conjugate heat transfer at Prandtl number 0.01. *Nucl. Eng. Des.*, 253:153–160, 2012. doi: 10.1016/j.nucengdes.2012.08.008.

[16] C. Flageul, S. Benhamadouche, É. Lamballais, and D. Laurence. DNS of turbulent channel flow with conjugate heat transfer: effect of thermal boundary conditions on the second moments and budgets. *Int. J. Heat Fluid Flow*, 55:34–44, 2015. doi: 10.1016/j.ijheatfluidflow.2015.07.009.

[17] H. Abe, R. A. Antonia, and H. Kawamura. Correlation between small-scale velocity and scalar fluctuations in a turbulent channel flow. *J. Fluid Mech.*, 627:1–32, 2009. doi: 10.1017/S0022112008005569.

[18] S. Pirozzoli, M. Bernardini, R. Verzicco, and P. Orlandi. Mixed convection in turbulent channels with unstable stratification. *J. Fluid Mech.*, 821:482–516, 2017. doi: 10.1017/jfm.2017.216.

[19] B. I. Shraiman and E. D. Siggia. Heat transport in high-Rayleigh-number convection. *Phys. Rev. A*, 42:3650–3653, 1990. doi: 10.1103/PhysRevA.42.3650.

[20] S. Grossmann and D. Lohse. Scaling in thermal convection: a unifying theory. *J. Fluid Mech.*, 407:27–56, 2000. doi: 10.1017/S0022112099007545.

[21] S. B. Pope. A more general effective-viscosity hypothesis. *J. Fluid Mech.*, 72:331–340, 1975. doi: 10.1017/S0022112075003382.

[22] J. Ling, A. Kurzawski, and J. Templeton. Reynolds averaged turbulence modelling using deep neural networks with embedded invariance. *J. Fluid Mech.*, 807:155–166, 2016. doi: 10.1017/jfm.2016.615.

[23] Deniz Günseren, Özgür Ertunç, Ismail Ari, Atakan Ataman Atik, Nitel Muhtaroglu, and Ivan Otić. Constructing a Reynolds stress model of decaying homogeneous isotropic turbulence using physics informed neural network. *J. Comput. Phys.*, 553:114725, 2026. doi: 10.1016/j.jcp.2026.114725.